

GLOBAL INTER--ANNUAL TRENDS AND AMPLITUDE MODULATIONS OF THE SEA SURFACE HEIGHT ANOMALY FROM THE TOPEX/JASON--1 ALTIMETERS

Paulo S. Polito* and Olga T. Sato
Instituto Oceanográfico da Universidade de São Paulo,
São Paulo, SP, Brazil

Abstract

This study uses the global TOPEX/Jason-1 altimeters time series to estimate the 12-year trends in: sea surface height anomaly, amplitude of the seasonal cycle of the sea surface height, amplitude of the Rossby and equatorial Kelvin wave signals, and meso- and small-scale eddies. The global distribution of these trends is discussed and a comparison of representative latitudes from the Atlantic, Pacific and Indian Oceans is presented. The inter-annual sea surface height trend shows large local variations over small regions where the intense western boundary currents turn. Such trends imply in a change of the cross-stream slope or a latitudinal shift in the mean current path, or both. These, in turn, lead to a change in the geostrophic velocity and its shear. In these regions significant amplitude trends are observed in the meso-scale eddy field, and, to a lesser degree, in the Rossby wave field. We hypothesize that the spatially inhomogeneous trends in sea surface height leads to changes in the local geostrophic transport and the mean position of the western boundary currents. This in turn affects the instability related processes that generate meso-scale eddies. Analysis of the linear trend in amplitude of the meso-scale eddies corroborates this hypothesis.

1. INTRODUCTION

The global time series of sea surface height (SSH) anomaly collected by the TOPEX and JASON-1 altimeters is now more than one decade long. This quasi-global SSH anomaly measurements are directly related to the heat storage variability (Chambers et al., 1997; Polito et al., 2000]), and therefore establish the connection between satellite altimetry and climate change studies. Although too short for the analysis of decadal and inter-decadal processes, statistically significant linear tendencies can be obtained from altimeter data. The proposed analysis of these tendencies is a method to investigate the dynamical consequences of the observed changes in SSH. No inferences are made regarding the periodicity or duration of these changes, given the length of the time series.

The sea level changes mostly because of thermohaline expansion, glacier ice, polar ice, ice

sheets, and terrestrial storage. Independent estimates that account for each of these major factors contributes with an error estimate that leads to a globally averaged total of 0.7 ± 1.5 mm/yr. Similar estimates obtained directly from tide gauges result in 1.5 ± 0.5 mm/yr; numerical climate models from the Intergovernmental Panel on Climate Change (IPCC) suggest values between 0.8 and 8 mm/yr; previous results derived from satellite altimeter data indicate 3.1 ± 0.4 mm/yr. All these results were presented and thoroughly discussed in Church et al. (2001) and Cazenave and Nerem (2004).

Regional variations in sea level change rate were observed in both hydrographic and satellite data (Cabanes et al., 2001). From a dynamical point of view, different rates of sea level change lead to a change of surface slope that, in turn, locally changes the geostrophic velocity field and its horizontal gradient. From a thermodynamical point of view, the spatially inhomogeneous rate of sea level change implies in local differences in the heat storage rate. These differences imply in localized variations in the temperature and, to a lesser degree, in the salinity throughout the water column (Sato and Rossby, 2000), and therefore, in horizontal density gradients. Back to the dynamics, through the thermal wind equations these gradients translate into vertical shear of horizontal velocities. In both cases, changes in the horizontal velocity gradient imply in changes in the basic elements that condition instability processes. Therefore we hypothesize that these long-term trends may have observable consequences in higher frequency bands.

The global SSH anomaly record is, in most latitudes, dominated by basin-scale signals that include the seasonal and inter-annual cycles (e.g. El Niño/La Niña, North Atlantic Oscillation, Indian Ocean Dipole etc.). The purely seasonal cycle has a fixed annual period, but its amplitude is variable. Signals characterized as long and short baroclinic Rossby waves (Chelton and Schlax, 1996; Polito and Cornillon, 1997; Cipollini et al., 1997) are the second most energetic in most of low and mid-latitudes, in addition to equatorial Kelvin waves (Polito et al., 2001). Rossby waves are present on the altimeter data record of the three basins in a variety of wavelengths and periods (Polito and Liu, 2003). These waves are predominantly

* Corresponding author address: Paulo S. Polito, Instituto Oceanográfico da Universidade de São Paulo, Pca.do Oceanográfico, 191, São Paulo, SP, Brazil, 05508-120; e-mail: polito@io.usp.br.

of the first baroclinic mode, and thus share the same dynamical framework. That, in turn, imposes a latitude dependent, westward phase speed, although periods and wavelengths may vary. Due to the dependence of the critical latitude on the wave frequency, the more poleward the latitude, the lower the Rossby wave frequency threshold imposed by the dynamics. As a result, relatively short period (~ 50 days) Rossby waves are found only in low latitudes (Polito and Liu, 2003); annual Rossby waves predominate in mid latitudes; and inter-annual Rossby waves reach their critical latitude near the Polar Circle. Consequently, in high latitudes most of the Rossby wave signal vanishes, while meso- and small-scale eddies gain amplitude (Polito and Liu, 2003, Figure 7). Furthermore, the total variability of the SSH is spatially inhomogeneous. There are local maxima over the regions where all major western boundary currents turn east, namely the Kuroshio, Gulf Stream, Agulhas and Brazil currents. In addition, local maxima are observed near the Antarctic circumpolar current and in the low latitudes of the Pacific and Indian Oceans.

The objectives of this study are to quantify and analyze the local inter-annual trends in satellite derived SSH of the: (a) total signal and the trends of the amplitude of the (b) seasonal cycle, (c) baroclinic Rossby and (d) Kelvin waves, and (e) meso- and small-scale eddies.

2. ALTIMETER DATA

The observational basis of this study is constructed from the TOPEX and JASON-1 altimeter data distributed by the Jet Propulsion Laboratory (JPL) Physical Oceanography Distributed Active Archive Center (PODAAC). The along-track interpolated geophysical data record is used, all standard corrections are applied (Benada, 1997).

The altimeter data has a sampling period of approximately 10 days (9.9156) and an equatorial track separation of 315 km in the zonal direction. The T/P data are interpolated (Smith and Wessel, 1990) into a regular $1^\circ \times 1^\circ \times 9.9156$ days and are called $h_o(x, y, t)$. A 12-year long time series of maps from August 1993 to August 2005 was assembled and reorganized into zonal-temporal (Hovmoller) diagrams of $h_o(x, t)$, one per degree of latitude. At each basin and latitude is band-pass filtered into several additive components using an improved version of the method used in Polito et al. (2000) and Polito and Liu (2003), briefly explained in Section 2.1.

2.1 Spectral Decomposition

The methodology applied in the analysis of $h_o(x, t)$ is the use of a sequence of two-dimensional finite impulse response filters (FIR-2D), similar to that described in Polito and Liu, (2003). The main improvement is that the present version is able to separate three bands of eastward propagating

equatorial Kelvin waves from the westward propagating Rossby waves, improving the signal-to-noise ratio in the Rossby wave bands. is decomposed into:

$$h_o = h_{24} + h_{12} + h_6 + h_3 + h_1 + \dots$$

$$\dots h_{K6} + h_{K3} + h_{K1} + h_E + h_r \quad (1)$$

h_i is the non-propagating, basin-scale signal and is dominated by seasonality and El Niño variability. In this case a two-dimensional symmetric Gaussian filter is used to capture temporal scales of one year or more and wavelengths similar to the local basin width.

$h_{24} \dots h_1$ are the westward propagating Rossby waves with approximate periods of 24, 12, 6, 3 and 1.5 months. The equatorial Kelvin wave signals,

$h_{K6} \dots h_{K1}$ are present only in the equatorial region and refer to Kelvin waves with approximate periods of 6, 3, and 1.5 months. A symmetric Gaussian filter is applied to the remaining non-propagating signal. It separates the meso-scale h_E from h_r , the small-scale residual. Each 2D FIR filter convolves a filter matrix with the data matrix to produce a band-pass filtered output. For both Kelvin and Rossby waves the filter matrices are Gaussian-tapered co-sinusoidal surfaces. The slope of these surfaces is associated with the phase speed of the waves in the pass-band. Therefore, the filter is able to distinguish not only eastward (positive slope) from westward (negative slope) propagation but also different phase speeds.

The filters are applied at each basin and latitude independently, in a sequence of decreasing periods and wavelengths. For each band the filtered output is removed from the remaining signal before the next filter is applied. The pass-band of these filters are broad by design, allowing for substantial variability in period and wavelength within each band. The bandwidth is such that there is a small overlap of adjacent bands, ensuring a complete coverage of the spectrum. Furthermore, although the periods are fixed, the wavelengths are iteratively adjusted towards the local maximum in amplitude. The data are processed globally, with a consistent methodology for all bands.

3. RESULTS AND DISCUSSION

The original altimeter signal is decomposed according to Equation . The non-propagating, basin-scale signal is dominated by seasonality and inter-annual variability. The the time series extends for exact 12 years, thus the phase of the annual cycle poses no problem to the determination of the long-term trend. The amplitude of the annual cycle varies, and this variation can be large enough, in some regions, to influence the long-term trend estimate. To avoid this effect, the local time series is smoothed with a simple low-pass filter that cuts off most of the annual and higher frequencies. A straight line is least-squares fit to this smooth curve, and the angular coefficient is regarded as the trend.

The global results obtained from this operation are shown in Figure 1 (a), top. The large scale features shown here are very similar to Figure 7 in Cazenave and Nerem, (2004). The discrepancies are attributed to the fact that, in this case, the data were filtered and, to a lesser degree, that the lengths of the time series are different. There are two marked locations in the Pacific at 34.5°N, 14.5°E and at 38.5°N, 14.5°E. At both of these places the overall trend is particularly high, yet it is negative at 38.5°N and positive at 34.5°N. This change in SSH trend over a relatively short distance is not particular to the Kuroshio region. Similar results are clearly seen over the Gulf Stream and, in a less intense way, in all other western boundary current systems. This extreme case of the Kuroshio is shown in detail in the top two plots of Figure 1. It is important to notice from the extent of the vertical axis that the overall SSH amplitude is relatively large (~2m) in this region. The thin line shows the seasonal signal, and it is clear that its variability occurs over a wide spectral range, with a significant amount of energy in the high-frequency bin. The FIR filtered basin-scale signal is shown in the slightly thicker line. In that, the seasonal signal is evident, particularly before 1997. This is an indication that the spectral composition of the signal is variable. The seasonal signal is removed with a simple low-pass filter, and the result is shown in a slightly thicker line. This smooth signal is the basin-scale inter-annual residual variability, and its long-term trend is evident. The thickest straight line is least-squares fit to this smooth signal. Above each of the plots there is the Basin, the location, the coefficient of determination R , the probability that this R can be obtained from random data and the angular coefficient of the straight line. In both cases a statistically significant trend is observed, with opposite signs.

The inspection of the seasonal signal on many locations revealed that the amplitude of the seasonal SSH variability often varies significantly. The energy input in the form of shortwave solar radiation has a nearly constant annual cycle. Thus, most of this amplitude variability is due to factors internal to the ocean-atmosphere system. Among those, the two major factors are the long wave radiation and the meridional oceanic heat flux. Different trends in the seasonal signal amplitude of relatively close locations imply that the annual variation of the slope, and thus the annual variation of the geostrophic currents are changing. To quantify the tendency of the amplitude of the seasonal cycle, the amplitude of the seasonal cycle, minus the smoothed basin-scale inter-annual variability (top two plots of Figure 2) previously obtained was used. This purely seasonal signal is shown as the thick curve in the second row of plots in Figure 2 for the Atlantic Ocean at 37.5°N, 49.5°W, and 41.5°N, 49.5°W. To quantify the amplitude modulation the absolute value of the time series was calculated (thin line) and the local maxima estimated (circles). Through these local maxima a straight line was least squares fit. Amplitude

modulations are evident from the misalignment of the circles, yet these modulations are not very well described by a straight line as shown by the coefficients of determination R of 0.56 and 0.38, respectively. The tendency itself is significant as is, in both cases, relatively small. In Figure 1 (b), the colored map shows the global distribution of this tendency. In general, the global trends of the amplitude of the seasonal cycle are less intense and less smooth than the long-term trend of the SSH. Furthermore, the latter is dominated by positive values (green, yellow and red regions in Figure 1 (a)), while the former shows more of an equilibrium between positive and negative trends. Large regions between 10° and 30° of the Atlantic and southeastern Pacific show nearly zero trend. Positive trends are observed in the equatorial Atlantic and Indian Oceans. In the Indian basin, between approximately 6° and 20° north and south a negative trend shows up as blue and purple colors. A similar observation is made in the South Pacific, however along 15°N a positive tendency is evident, and spreads from the western boundary to the dateline, and from Central America to approximately 120°W. Large positive and negative tendencies are observed in mid latitudes as zonally elongated regions over the major western boundary extensions. The previously discussed results over locations in the Gulf Stream region are marked in Figure 1 (b). Similar patterns are observed in the Kuroshio and Agulhas regions. Over the western south Atlantic, between 30°S and 45°S, there is a general tendency of decrease in amplitude.

The same method used to obtain the long-term trend of the annual cycle was used to estimate the trend of the amplitude of baroclinic Rossby waves. For that the sum of the FIR-filtered Rossby wave components is calculated, and a straight line is fit on the local maxima of the absolute value of the signal. This operations are performed in all grid points between the critical latitudes of the lowest frequency waves. The global distribution of these trends is shown in Figure 1 (c). In comparison with the seasonal signal amplitude trend (Figure 1 (b)), the Rossby waves amplitude trend reaches higher values over wider areas. Continuous patterns often cover relatively larger regions (i.e. the signal is less patchy). The trend in the Atlantic between 5°N and the tropic of Capricorn is approximately zero. Poleward of 30°, in all basins, a positive trend is observed. In the North Atlantic this limit is approximately 20°N. Significant positive trends are also found over large regions of the northwestern Pacific and southwestern Indian Oceans. Localized maxima occur, as in the two cases above, in the vicinity of western boundary currents and their zonal extensions. Negative trends are observed over a wide region in the Pacific Ocean, approximately between 5°N to 30°S, and 150°E to 120°W. Two examples of significant trends are shown in third row of plots of Figure 2, one for 39.5°S, 36.5°E, in the Indian Ocean, and one for 29.5°S, 30.5°W, in the Atlantic Ocean.

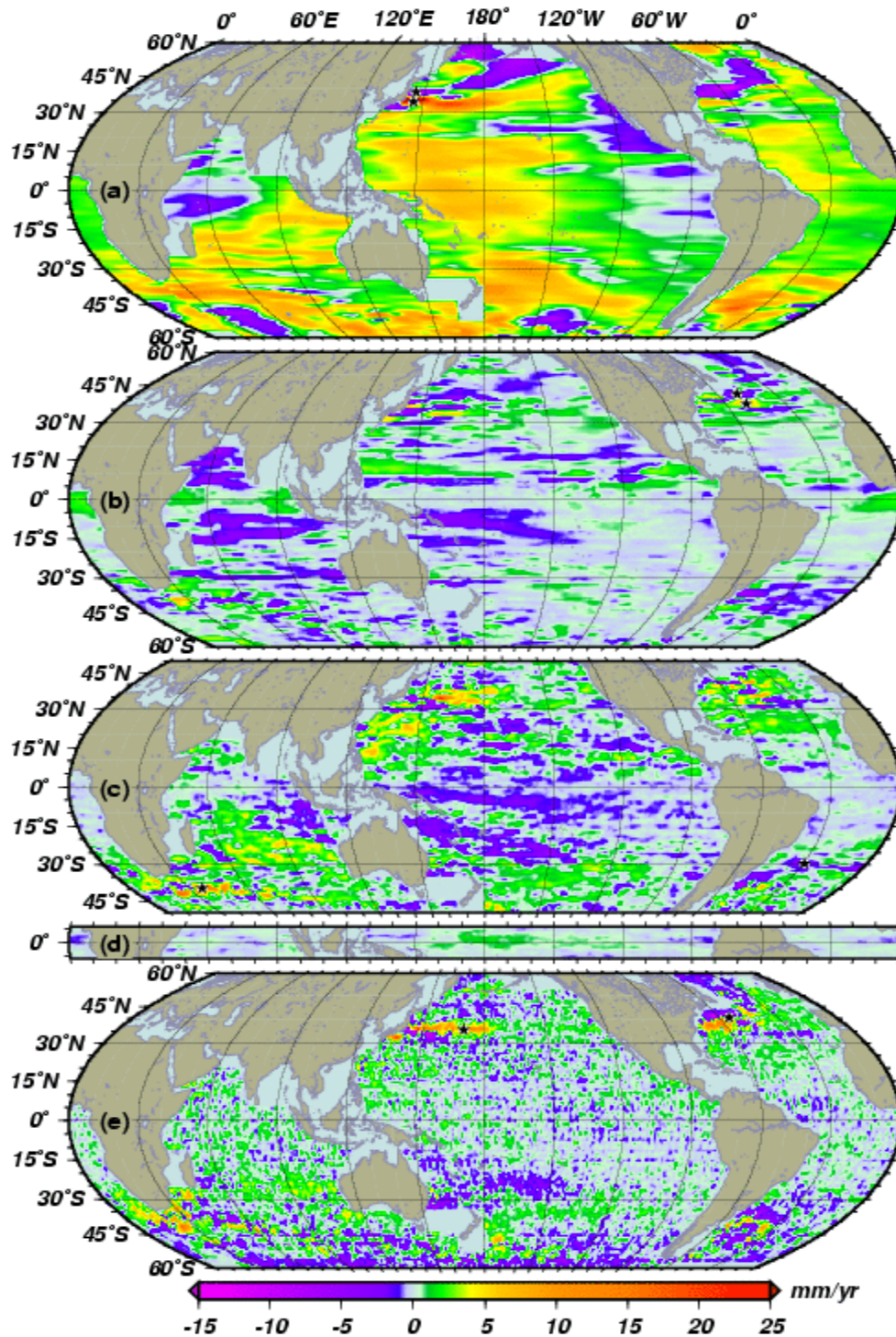


Figure 1: Global distribution of altimeter-derived SSH trends: (a) overall long-term trend; (b) trend of the amplitude of the annual cycle; (c) trend of the amplitude of the first-mode baroclinic Rossby waves; (d) trend of the amplitude of the equatorial Kelvin waves; (e) trend of the amplitude of the meso- and small-scale eddies; all in mm/year. Areas shallower than 1000m and small zonally enclosed regions are excluded because of the filtering process. The time series at the marked locations are seen in detail in Figure 2.

The values of R , 0.48 and 0.43 respectively, are not impressive and indicate that the trends are not well described by a straight line. However, the probability of a random set with equal number of degrees of freedom generate such trends is minimal, 0.44% and 0.10%.

Similar to the Rossby wave data processing, the equatorial Kelvin wave field is the sum of the eastward propagating signals obtained from the FIR-filters. The global results for the trend in amplitude of equatorial Kelvin waves are shown in Figure 1 (d). In general, the amplitude tendency is approximately zero, except for the central equatorial Pacific, that shows a slight positive trend. In addition, the analysis is limited by the filter performance, which in this spectral band is not as good as in the Rossby waves case (Polito et al., 2000).

The basin-scale non-propagating signals, plus Rossby and Kelvin wave components are subtracted from the original altimeter record. The residual contains meso- and small-scale signals that do not propagate as equatorial Kelvin or Rossby waves. Although their origin and dynamics are beyond the scope of this study, this spectral band includes also the high-frequency part of the instrument noise and possibly aliased tide residuals. The tendency of the amplitude of the eddy signals is estimated through the same method as the previous amplitude trends. Figure 1 (e) shows a map of the global distribution of the amplitude trend. The granular patterns that appear over most of Figure 1 (e) are identified as noise and thus not analyzed. In most of the area between 40°S and 40°N the amplitude of the eddy field has increased in the last 12 years. Negative trends are observed mostly in high latitudes, except for the southwestern Pacific, between the coast of Australia and the 150°W meridian, where negative values extend north up to 15°S. Significant trends are observed as continuous patches that extend zonally in the vicinity of the eastward extension of the major western boundary currents. These regions show alternating patches of positive and negative amplitude trends. The marked locations, 35.5°N, 169.5°E (Kuroshio) in the Pacific, and 40.5°N, 54.5°W (Gulf Stream) in the Atlantic, are shown in detail in the last row of Figure 2, and follow the same line convention. The coefficients of determination R are relatively small, 0.29 and 0.41, respectively. Although the total tendencies are small compared to the maximum amplitude of the signal, the number of degrees of freedom are large, because of the high frequency. Therefore, the probabilities that this adjust occurs out of random chance are small, 1.68% and 0.04%, respectively.

4. Conclusions

The decomposition of the altimeter signal allowed for an advance in the interpretation of the long term variability of the satellite based sea surface height record. Two different trends are analyzed. The first is the long term trend of the sea surface height. In this

study, different from (), the trend was calculated using only the basin-scale, non-propagating, non-seasonal, part of the altimetric spectrum. The basin-scale, non-propagating signal was obtained from a method based on 2D finite impulse response filters (). The seasonal signal was removed by locally passing a simple band-pass filter to eliminate as much as possible the signals whose period is one year or less. A straight line was fit to this smooth curve and the angular coefficient is taken as the 12-years trend. Meso- and small- scale eddies, propagating Rossby and equatorial Kelvin waves and seasonal signals were analyzed through a second type of trend. These signals are inherently transient, and the long-term trend in the amplitude between adjacent maxima and minima was estimated. If, for example, the waves become more and more intense, this trend will be positive. Otherwise, if the waves tend to vanish, this trend will be negative. Figure 1 shows the global distribution of these trends. The top map (a) shows the long-term trend of the basin-scale non-propagating, non-seasonal signal. In general, it is very similar to the results in Cazenave and Nerem (2004). Trends are, in a global average, positive as expected from previous results. This positive trend is more predominant over the southern hemisphere.

Local extrema in the long-term trend shown in Figure 1(a) occur over all major western boundary currents, more specifically in the regions where the currents turn to the east. In these regions, maxima of opposite signs are often found within a few degrees of latitude of each other. This means that, in 12 years, one side of the current has increased in height and the other side decreased. An extreme case occurs in the Kuroshio/Oyashio region and is shown in detail in the top row of Figure 2. The more plausible explanations for such a large change in slope are the intensification and northward shift in the path of the current, probably associated with a change in the large-scale wind stress curl (Seager et al., 2001; Qiu, 2002; Ezer, 1999; Frankignoul et al., 2002). In spite of the relatively low spatial resolution of the altimeter data compared to the mean width of the current, the positive and negative regions consistently spread over a large area. The FIR filters could influence the zonal dimension, but not the meridional dimension because they are applied to the Hovmöller diagrams, and each latitude is filtered independently of the others. Thus, given the continuous extent of the positive and negative regions, they are very probably of geophysical origin.

The trend of the amplitude of the seasonal cycle shown in Figure 2 (b). The trends are, in average, smaller in absolute value than the long-term trends discussed above, and there is more of a balance between positive and negative trends. Positive trends dominate in the equatorial Indian and Atlantic Oceans, and in the Pacific positive trends occur in the vicinity of 10°N. Between approximately 5 and 20 the Indian Ocean shows a relatively large and consistent negative trend. This suggests that the annual variation of the

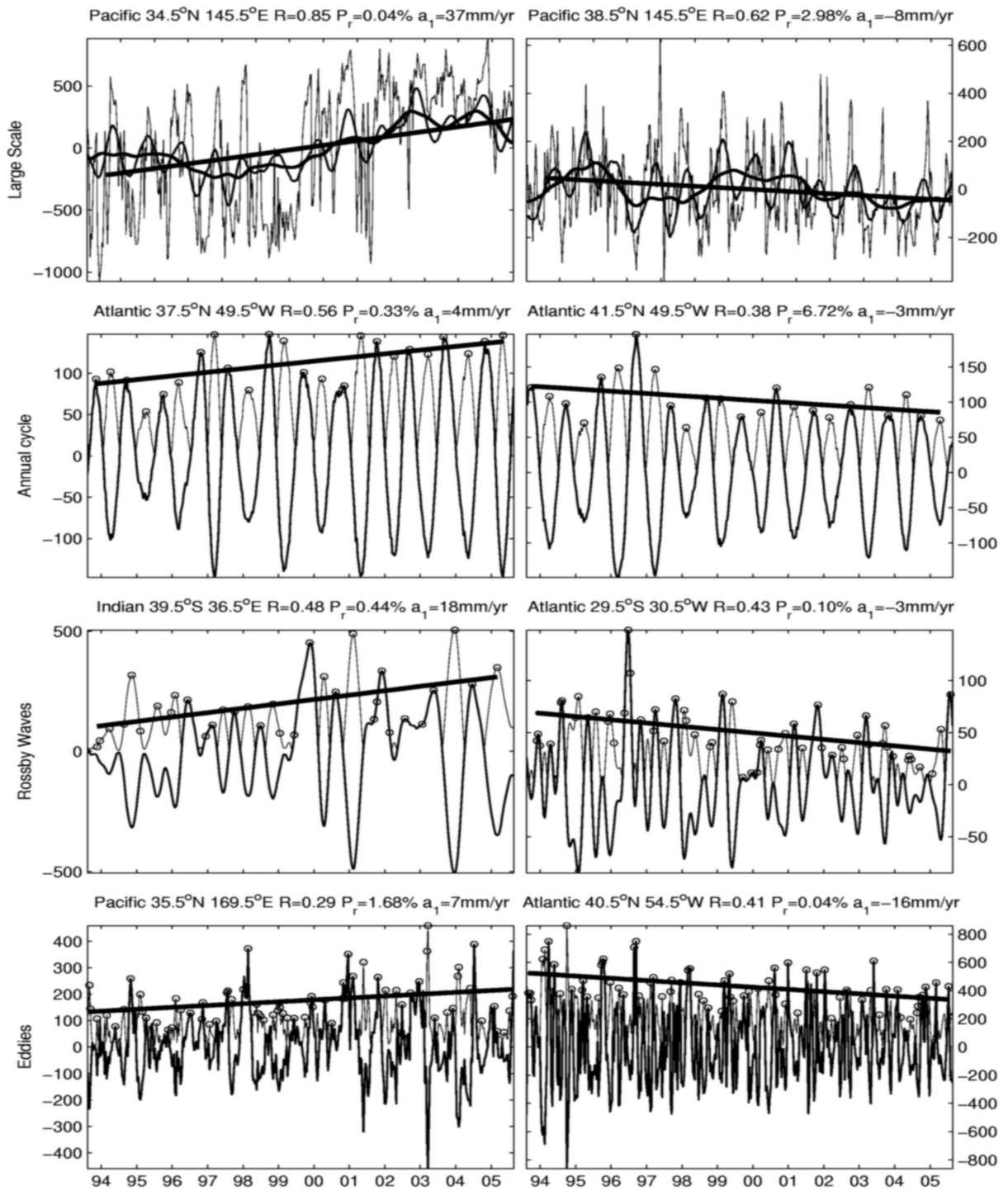


Figure 2: The plots in this figure correspond to the marked locations in Figure 1. Above each plot there is the basin name, location, coefficient of determination, probability of a random data set to yield such coefficient and the trend. The vertical axis shows the height anomaly in mm and the horizontal axis shows the time in years. In the first row of plots the thinnest line shows the original altimetric time series, the second most thin shows the non-propagating, basin-scale signal h_t , the third shows the smoothed h_t with the seasonal cycle removed and the thickest line shows the linear trend. In second row of plots the thick line shows the de-trended annual cycle; the thin line shows its absolute value; the circles mark the local maxima and the thick line shows the linear trend of the amplitude. Similarly, the third and fourth rows show results for the total Rossby wave signal and the meso- and small-scale eddies.

heat storage in this region is decreasing. One can speculate that either the seasonal surface flux follows the same trend or that the seasonal thermocline is progressively shallower.

Zonally elongated local maxima of opposite signs are observed (Figure 1 (b)) in the regions where western boundary currents turn to the east. This is interpreted as a result of the lateral movement of the mean current paths. The geostrophic transport of all major western boundary currents varies seasonally, and so does the cross-stream slope. A latitudinal shift in the currents path would locally change this seasonal cycle, increasing its amplitude on one side and decreasing it on the other. It is interesting to notice that in the second row of Figure 2, at both marked locations, the annual cycle amplitude goes from a more variable state in the first 7 to 8 years of the time series, to a more stable state in more recent years. This is clearly outside the reach of a simple linear trend analysis, however it is a potentially interesting feature to analyze with a longer time series.

The trend of the amplitude of the Rossby wave field is shown in Figure 2 (c). In contrast with the previous case, nearly continuous regions cover relatively large regions. Positive trends are observed globally, in latitudes higher than approximately 30 (20°N the North Atlantic). In addition, significant positive trends are observed in the northwestern Pacific and southwestern Indian Oceans. A large region with negative trends occupies the central south Pacific. As a whole, positive trends dominate both in area and in intensity. More intense positive trends are found in the western half of the basins, in mid latitudes (Figure 1, third row). In this case, local maxima are not necessarily tied to the exact position of the western boundary currents, but spread over a much larger area. Figure 2 (d) shows the trends of the amplitude of Equatorial Kelvin waves. In most regions this trend is nearly zero, except for the central Pacific, where it is positive.

The trend of the amplitude calculated based on the spectral band identified as meso- and small-scale eddies is shown in Figure 1 (e). Although this spectral band includes noise from several sources, residual tides, and non-resolved geophysical signals in addition to the meso- and small-scale eddies, its analysis can still provide some self-consistent information. Most of the Indian Ocean, North Atlantic, and North Pacific show small, predominantly positive trends. Negative trends are observed mostly in high latitudes and mostly in the southern hemisphere. In each basin, local maxima/minima occur exactly in the region where the most intense western boundary currents veer to the east. This is an indication of a meridional shift in the mean position of the currents, and of the meanders and eddies that it generates.

The present observations indicate a predominantly positive tendency in the amplitude of both Rossby and equatorial Kelvin waves, and to a lesser degree, of meso- and small-scale eddies. These observations

suggest that these transient events are, in a global average, becoming more energetic. In some regions, the variation in amplitude over 12 years is comparable to the standard deviation of the data and is statistically significant (Figure 2).

Rossby and Kelvin waves can be generated by atmospheric forcing and, as for the eddies, by instability processes. An increase in atmospheric variability (Easterling et al. 2000) would introduce more energy into the ocean. This study presents evidences that suggest that the most intense currents are changing in position, in intensity or both. This in turn changes the velocity shear that potentially influences instability processes and thus more transient signals have been generated in the last 12 years.

Acknowledgements

We would like to thank the support from the *Fundação para Amparo à Pesquisa do Estado de São Paulo* (FAPESP) under project 01/06921-3.

References

- Benada, R. (1997). *Merged GDR TOPEX/Poseidon Users Handbook Version 2.0*. Jet Propulsion Lab. PO.DAAC. D-11007.
- Cabanes, C., Cazenave, A., and Provost, C. L. (2001). Sea level rise during past 40 years determined from satellite and in situ observations. *Science*, 294:840–842.
- Cazenave, A. and Nerem, R. S. (2004). Present-day sea level change: Observations and causes. *Reviews of Geophysics*, 42. RG3001.
- Chambers, D. P., Tapley, B. D., and Stewart, R. H. (1997). Long-period ocean heat storage rates and basin-scale heat fluxes from TOPEX. *Journal of Geophysical Research*, 102(C5):10,525–10,533.
- Chelton, D. B. and Schlax, M. (1996). Global observations of oceanic Rossby waves. *Science*, 272:234–238.
- Church, J., Gregory, J. M., Huybrechts, P., Kuhn, M., Lambeck, K., Nhuan, M. T., Qin, D., and Woodworth, P. L. (2001). *Changes in sea level, in Climate Change 2001: The Scientific Basis, Contribution of Working Group I to the Third Assessment Report of the Intergovernmental Panel on Climate Change*. Cambridge Univ. Press, New York. pp. 639–693.
- Cipollini, P., Cromwell, D., Jones, M. S., Quartly, G. D., and Challenor, P. G. (1997). Concurrent altimeter and infrared observations of Rossby wave propagation near 34N in the northeast Atlantic. *Geophysical Research Letters*, 24:889–892.
- Easterling, D. R., Evans, J. L., Groisman, P. Y., Karl, T. R., Kunkle, K. E., and Ambenje, P. (2000). Observed variability and trends in extreme climate events: a brief review. *Bulletin of the American Meteorological Society*, 81(3):417–425.
- Ezer, T. (1999). Decadal variabilities of the upper layers of the subtropical north atlantic: An ocean model study. *Journal of Physical Oceanography*,

- 29(12):3111–3124.
- Frankignoul, C., de Coëtlogon, G., Joyce, T. M., and Dong, S. (2002). Gulf Stream variability and ocean–atmosphere interactions. *Journal of Physical Oceanography*, 31(12):3516–3529.
- Polito, P. S. and Cornillon, P. (1997). Long baroclinic Rossby waves detected by TOPEX/Poseidon. *Journal of Geophysical Research*, 102:3215–3235.
- Polito, P. S. and Liu, W. T. (2003). Global characterization of Rossby waves at several spectral bands. *Journal of Geophysical Research*, 108(C1). 3018, doi: 10.1029/2000JC000607.
- Polito, P. S., Ryan, J. P., Liu, W. T., and Chavez, F. P. (2001). Oceanic and atmospheric anomalies of tropical instability waves. *Geophysical Research Letters*, 28(11):2233–2236.
- Polito, P. S., Sato, O. T., and Liu, W. T. (2000). Characterization and validation of heat storage variability from TOPEX/Poseidon at four oceanographic sites. *Journal of Geophysical Research*, 105(C7):16,911–16,921.
- Qiu, B. (2002). The Kuroshio extension system: Its large-scale variability and role in the midlatitude ocean–atmosphere interaction. *Journal of Oceanography*, 58:57–75.
- Sato, O. T. and Rossby, T. (2000). Seasonal and low frequency variability in the meridional heat flux at 36N in the North Atlantic. *Journal of Physical Oceanography*, 30(3):606–621.
- Seager, R., Kushnir, Y., Naik, N. H., Cane, M. A., and Miller, J. (2001). Wind-driven shifts in the latitude of the Kuroshio–Oyashio extension and generation of SST anomalies on decadal timescales. *Journal of Climate*, 14(22):4249–4265.
- Smith, W. H. F. and Wessel, P. (1990). Gridding with a continuous curvature surface in tension. *Geophysics*, 55:293–305.